Article

Oxide and Carbide Formation at Titanium/Organic Monolayer Interfaces

Jason J. Blackstock, Carrie L. Donley, William F. Stickle, Douglas A. A. Ohlberg, J. Joshua Yang, Duncan R. Stewart, and R. Stanley Williams

J. Am. Chem. Soc., **2008**, 130 (12), 4041-4047 • DOI: 10.1021/ja710448e

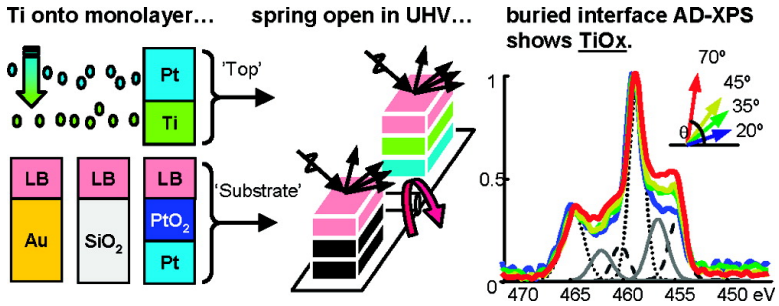

More About This Article

Additional resources and features associated with this article are available within the HTML version:

- Supporting Information
- Links to the 1 articles that cite this article, as of the time of this article download
- Access to high resolution figures
- Links to articles and content related to this article
- Copyright permission to reproduce figures and/or text from this article

View the Full Text HTML

J|A|C|S
ARTICLES
Published on Web 03/05/2008

Oxide and Carbide Formation at Titanium/Organic Monolayer Interfaces

Jason J. Blackstock,[†] Carrie L. Donley,[†,§] William F. Stickle,[‡] Douglas A. A. Ohlberg,[†] J. Joshua Yang,[†] Duncan R. Stewart,*[,†] and R. Stanley Williams[†]

Information and Quantum Systems Laboratory, Hewlett-Packard Laboratories, 1501 Page Mill Road, Palo Alto, California 94304, and Analytical and Development Laboratories, Hewlett-Packard Company, Corvallis, Oregon 97330

Received November 19, 2007; E-mail: duncan.stewart@hp.com

Abstract: X-ray photoelectron spectra (XPS) are reported from a series of buried titanium/organic monolayer interfaces accessed through sample delamination in ultrahigh vacuum (UHV). Conventional characterization of such buried interfaces requires ion-mill depth profiling, an energetic process that frequently destroys bonding information by chemically reducing the milled material. In contrast, we show that delaminating the samples at the metal/organic interface in vacuum yields sharp, nonreduced spectra that allow quantitative analysis of the buried interface chemistry. Using this UHV delamination XPS, we examine titanium vapor deposited onto a C_{18} cadmium stearate Langmuir−Blodgett monolayer supported on Au, SiO_2, or PtO_2 substrates. Titanium is widely used as an adhesion layer in organic thick film metallization as well as a top metal contact for molecular monolayer junctions, where it has been assumed to form a few-atoms-thick Ti carbide overlayer. We establish here that under many conditions the titanium instead forms a *few-nanometers-thick Ti oxide* overlayer. Both TiO_2 and reduced TiO_x species exist, with the relative proportion depending on oxygen availability. Oxygen is gettered during deposition from the ambient, from the organic film, and remarkably, from the substrate itself, producing substrate-dependent amounts of Ti oxide and Ti carbide "damage". On Au substrates, up to 20% of the molecular-monolayer carbon formed titanium carbide, SiO_2 substrates ~15%, and PtO_2 substrates <5%. Titanium oxide formation is also strongly dependent on the deposition rate and chamber pressure.

Introduction

The chemistry of metal/organic interfaces formed by metal vapor deposition onto organic thin films has received considerable attention because of its rich kinetics and wide range of technology applications in organic and molecular electronics.[1−5] Obtaining accurate chemical information from such buried metal/organic interfaces is, however, notoriously difficult. In situ deposition/characterization systems are rare. "Backside" infrared studies of buried monolayers[6,7] are qualitatively very useful but difficult to make quantitative. Conventional spectroscopic analysis including X-ray photoelectron spectroscopy (XPS), Auger electron spectroscopy, or time-of-flight mass spectroscopy mandates energetic ion milling of the sample to mechanically drill down to the buried interface. Ion milling is known to destroy chemical bonding information by damaging the sample several nanometers into the exposed surface, often reducing it chemically. Spectra from critical nanometer-thick films and interfaces can easily be lost in the damaged background. In contrast, we report XPS data acquired from pristine internal metal/organic interfaces accessed through sample delamination in ultrahigh vacuum (UHV). We show by direct comparison to ion-milled data that delaminating at the metal/organic interface in vacuum produces sharp, nonreduced spectra that enable quantitative analysis of the interface chemistry. We use this UHV delamination XPS technique to study the reaction of vapor deposited titanium with organic Langmuir−Blodgett (LB) monolayers supported by Au, SiO_2, and PtO_2 substrates.

Titanium is both an archetype for highly reactive metals and important in its own right as a common adhesion layer for device metallization. Many recent electronic transport investigations of organic monolayers have also used Ti as a top contact metal.[6−17] Extensive previous work has shown the metal/organic interface chemistry to be strongly dependent on both the

[†] Hewlett-Packard Labs.
[‡] Hewlett-Packard Co.
[§] Current address: Institute for Advanced Materials, University of North Carolina, 243 Chapman Hall, Chapel Hill, NC 27599.

(1) Forrest, S. R.; Thompson, M. E. *Chem. Rev.* **2007**, *107*, 923.
(2) *Organic Electronics: Materials, Manufacturing, and Applications;* Klauk, H., Ed.; Wiley-VCH: Weinheim, Germany, 2006.
(3) *Molecular Electronics: A 'Chemistry for the 21st century';* Jortner, J., Ratner, M., Eds.; Blackwell Science: Malden, MA, 1997.
(4) *Molecular Nanoelectronics;* Reed, M. A., Lee, T., Eds.; American Scientific Publishers: Stevenson Ranch, CA, 2003.
(5) *Introducing Molecular Electronics;* Cuniberti, G., Fagas, G., Richter, K., Eds.; Springer, Berlin, 2005.
(6) (a) Richter, C. A.; Hacker, C. A.; Richter, L. J. *J. Phys. Chem. B* **2005**, *109*, 21836. (b) Hacker, C. A.; Richter, C. A.; Gergel-Hackett, N.; Richter, L. J. *J. Phys. Chem. C* **2007**, *111*, 9384.
(7) Donley, C. L.; Blackstock, J. J.; Stickle, W. F.; Stewart, D. R.; Williams, R. S. *Langmuir* **2007**, *23*, 7620.
(8) Collier, C. P.; Wong, E. W.; Belohradsky, M.; Raymo, F. M.; Stoddart, J. F.; Kuekes, P. J.; Williams, R. S.; Heath, J. R. *Science* **1999**, *285*, 391.

reactivity of the evaporated metal and the terminal chemistry of the monolayer. Outcomes range from completely displaced monolayers, to highly damaged or destroyed monolayers due to the formation of metal carbides, to nonpenetrating metal overlayers covalently bound to the terminal surface of the monolayer.[18−33] UHV studies of Ti deposition onto organic monolayers have widely reported TiC formation that consumes anywhere from a few C atoms to the full monolayer, then subsequent Ti aggregation and deposition as a metallic overlayer.[18,23,26,29,31,32] We find, however, that Ti often deposits onto organic monolayers as a few-nanometers-thick *Ti oxide* overlayer with a minor TiC component. The relative proportion of TiO_x and TiC is strongly affected by the substrate, and oxygen-rich PtO_2 substrates yield more TiO_2 and less TiC. Oxygen-poor Au substrates show little TiO_2 but more TiC. Ti oxide formation is also strongly affected by the deposition chamber ambient and the deposition rate. Few previous studies have examined these important roles of the substrate[6,7] and the deposition conditions[31] in the interface chemistry outcome. We establish these to be the dominant contributions determining interface chemistry in our system. This has significant implications for the many titanium-contacted molecular electronic transport measurements already reported in the literature, some of which may need to be reinterpreted.

Experimental Section

The organic monolayer junctions examined in this study were fabricated using standard procedures, as previously described in connection with several detailed electrical studies.[12,13,15] Briefly, three different material surfaces were employed as the bottom electrode. In the case of the Au and PtO_2 surfaces, the substrates were prepared by sputter-depositing a 100-nm film of Au or Pt onto Si(100) wafers previously coated with 100 nm of high-temperature thermal oxide. Both the Au and Pt surfaces were then treated with oxygen plasma immediately before the deposition of the cadmium stearate organic monolayer by the LB technique. Previous investigations[34,35] have revealed that, in addition to cleaning away adsorbed surface contaminants, the oxygen plasma treatment also creates an ultrathin (∼2.5 nm) platinum oxide layer on the Pt surface, composed mainly of PtO_2. No oxide formation on the Au surface was observed when measured by contact angle, ellipsometry, and XPS. For the silicon oxide substrate, the Si(100) wafers with 100-nm thermal oxide were used, and before the LB deposition of the cadmium stearate monolayer the silicon oxide surface was treated with the same oxygen plasma cleaning treatment as the two metal surfaces; no physical or chemical changes in the silicon oxide were observed by contact angle, ellipsometry, and XPS. The LB films of stearic acid were formed on a ∼1 mM cadmium chloride subphase, allowed to equilibrate for 30 min while the $CHCl_3$ solvent evaporated, compressed to 10 mN/m, expanded to a pressure of ∼1 mN/m (just past the liquid-condensed/liquid-expanded phase transition), and recompressed to 30 mN/m for transfer to the substrate.

Immediately following the deposition of the LB film, samples were transferred into the high vacuum electron beam metal deposition chamber (CHA Industries), and the titanium metal overlayer of 5 nm was deposited at a chamber pressure of $\sim 1 \times 10^{-6}$ Torr and a titanium evaporation rate of 0.01 nm/s (as measured by a quartz crystal monitor). Immediately following the titanium overlayer, without breaking the vacuum, a capping layer of platinum was deposited to prevent oxidization of the titanium by the ambient atmosphere; the platinum was deposited in sequential stages of 0.01 nm/s for the first 5 nm, 0.05 nm/s for the next 10 nm, and 0.1 nm/s for the remainder to a total thickness of 50 nm for the platinum layer. These three sample structures are illustrated in Figure 1a. To control for process variations in the bottom electrode and LB film structure, the Au, Pt, and SiO_2 substrate surfaces were prepared on different 1/4-in. square regions of a single large area silicon substrate, a single LB film was transferred to cover this entire prepatterned $Au/SiO_2/PtO_2$ surface, and the Ti + Pt top metallization was deposited over this full sample area.

The junctions were prepared for XPS characterization by first affixing the silicon substrate and top metal, respectively, to opposite faces of a spring-loaded hinge mechanism using epoxy. The spring mechanism was then inserted into the load-lock of the XPS system (PHI Quantera). The load-lock was evacuated, purged with nitrogen, then pumped to $<10^{-7}$ Torr. After the gate valve was opened to the main UHV chamber ($<10^{-8}$ Torr), the spring hinge was tripped to delaminate (strip) the sample. All devices delaminated at the organic monolayer, as shown schematically in Figure 1. This in situ delamination technique enables the collection of undistorted XPS data from *both* exposed surfaces of the delaminated interface, allowing chemical and physical characterization of this previously inaccessible buried interface. Angle-dependent XPS data were acquired using a 200-μm diameter area and monochromatic Al Kα X-rays, with the electron detector at an angle of 20°, 35°, 45°, or 70° to the sample surface plane. Depth profile ion milling was executed with 1 kV Ar ions during Zalar sample rotation. Spectra were charge-corrected to C(1s) at 284.8 eV.

Results

The sample structures and delamination process are illustrated schematically in Figure 1. Comparison of the Au, Si, Pt, Ti,

(9) Collier, C. P.; Mattersteig, G.; Wong, E. W.; Luo, Y.; Beverly, K.; Sampaio, J.; Raymo, F. M.; Stoddart, J. F.; Heath, J. R. *Science* **2000**, *289*, 1172.
(10) Chen, Y.; Ohlberg, D. A. A.; Li, X.; Stewart, D. R.; Jeppesen, J. O.; Nielsen, K. A.; Stoddart, J. F.; Olynick, D. L.; Anderson, E. *Appl. Phys. Lett.* **2003**, *82*, 1610.
(11) Chen, Y.; Jung, G.-Y.; Ohlberg, D. A. A.; Li, X.; Stewart, D. R.; Jeppesen, J. O.; Nielsen, K. A.; Stoddart, J. F.; Williams, R. S. *Nanotechnology* **2003**, *14*, 462.
(12) Lau, C. N.; Stewart, D. R.; Williams, R. S.; Bockrath, M. *Nano Lett.* **2004**, *4*, 569.
(13) Stewart, D. R.; Ohlberg, D. A. A.; Beck, P. A.; Chen, Y.; Williams, R. S.; Jeppesen, J. O.; Nielsen, K. A.; Stoddart, J. F. *Nano Lett.* **2004**, *4*, 133.
(14) Stewart, D. R.; Ohlberg, D. A. A.; Beck, P. A.; Lau, C. N.; Williams, R. S. *Appl. Phys. A* **2005**, *80*, 1379.
(15) Lau, C. N.; Stewart, D. R.; Bockrath, M.; Williams, R. S. *Appl. Phys. A* **2005**, *80*, 1373.
(16) Wu, W.; Jung, G.-Y.; Olynick, D. L.; Straznicky, J.; Li, Z.; Li, X.; Ohlberg, D. A. A.; Chen, Y.; Wang, S.-Y.; Liddle, J. A.; Tong, W. M.; Williams, R. S. *Appl. Phys. A* **2005**, *80*, 1173.
(17) Kuekes, P. J.; Stewart, D. R.; Williams, R. S. *J. Appl. Phys.* **2005**, *97*, 034301.
(18) Konstandinidis, K.; Zhang, P.; Opila, R. L.; Allara, D. L. *Surf. Sci.* **1995**, *338*, 300.
(19) Herdt, G. C.; Jung, D. R.; Czanderna, A. W. *Prog. Surf. Sci.* **1995**, *50*, 103.
(20) Jung, D. R.; Czanderna, A. W.; Herdt, G. C. *J. Vac. Sci. Technol., A* **1996**, *14*, 1779.
(21) Hooper, A.; Fisher, G. L.; Konstadinidis, K.; Jung, D.; Nguyen, H.; Opila, R.; Collins, R. W.; Winograd, N.; Allara, D. L. *J. Am. Chem. Soc.* **1999**, *121*, 8052.
(22) Fisher, G. L.; Walker, A. V.; Hooper, A. E.; Tighe, T. B.; Bahnck, K. B.; Skriba, H. T.; Reinard, M. D.; Hayie, B. C.; Opila, R. L.; Winograd, N.; Allara, D. L. *J. Am. Chem. Soc.* **2002**, *124*, 5528.
(23) Chang, S.-C.; Li, Z.; Lau, C. N.; Larade, B.; Williams, R. S. *Appl. Phys. Lett.* **2003**, *83*, 3198.
(24) Haynie, B. C.; Walker, A. V.; Tighe, T. B.; Allara, D. L.; Winograd, N. *Appl. Surf. Sci.* **2003**, *203−204*, 433.
(25) Walker, A. V.; Tighe, T. B.; Cabarcos, O. M.; Reinard, M. D.; Haynie, B. C.; Uppili, S.; Winograd, N.; Allara, D. L. *J. Am. Chem. Soc.* **2004**, *126*, 3954.
(26) Walker, A. V.; Tighe, T. B.; Stapleton, J.; Haynie, B. C.; Upilli, S.; Allara, D. L.; Winograd, N. *Appl. Phys. Lett.* **2004**, *84*, 4008.
(27) Jun, Y.; Zhu, X. Y. *J. Am. Chem. Soc.* **2004**, *126*, 13224.
(28) deBoer, B.; Frank, M. M.; Chabal, Y. J.; Jiang, W.; Garfunkel, E.; Bao, Z. *Langmuir* **2004**, *20*, 1539.
(29) Walker, A. V.; Tighe, T. B.; Haynie, B. C.; Uppili, S.; Winograd, N.; Allara, D. L. *J. Phys. Chem. B* **2005**, *109*, 11263.
(30) Nowak, A. M.; McCreery, R. L. *J. Am. Chem. Soc.* **2004**, *126*, 16621.
(31) McGovern, W. R.; Anariba, F.; McCreery, R. L. *J. Electrochem. Soc.* **2005**, *152*, E176.
(32) Tighe, T. B.; Daniel, T. A.; Zhu, Z.; Uppili, S.; Winograd, N.; Allara, D. L. *J. Phys. Chem. B* **2005**, *109*, 21006.
(33) Zhu, Z.; Daniel, T. A.; Maitani, M.; Cabarcos, O. M.; Allara, D. L.; Winograd, N. *J. Am. Chem. Soc.* **2006**, *128*, 13710.
(34) Li, Z.; Beck, P.; Ohlberg, D. A. A.; Stewart, D. F.; Williams, R. S. *Surf. Sci.* **2003**, *529*, 410.
(35) Blackstock, J. J.; Stewart, D. R.; Li, Z. *Appl. Phys. A* **2005**, *80*, 1343.

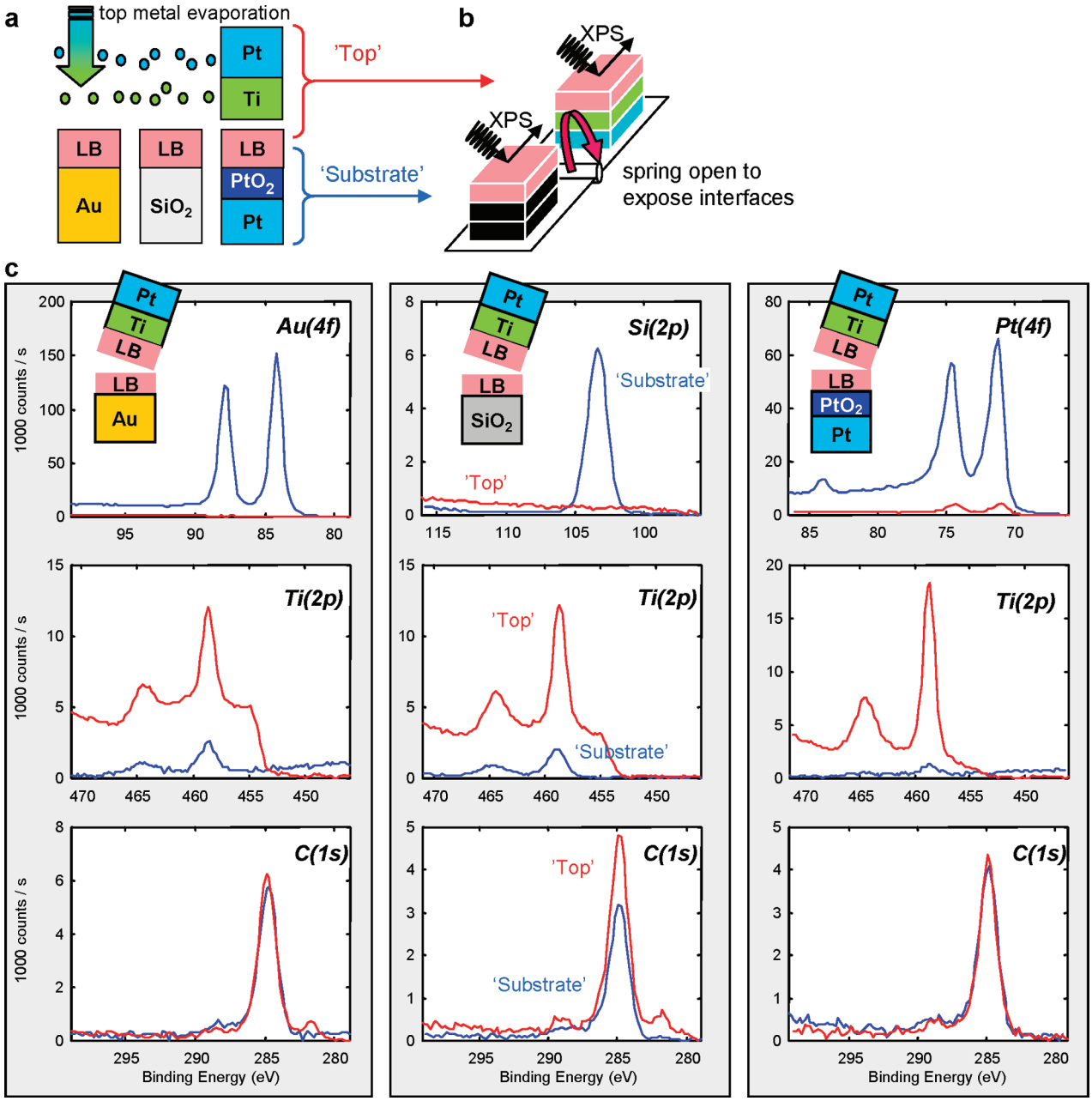

Figure 1. (a) Sample fabrication and characterization process: (left) Metallization by e-beam evaporation of metal onto the organic monolayer surface (0.1 A/s, $\leq 1 \times 10^{-6}$ Torr). (b) After loading into high vacuum (10^{-7} Torr) force is applied via a spring-loaded hinge to delaminate ("strip") the device structures ~5 s before transfer into UHV ($\leq 10^{-8}$ Torr). This enables clean photoemission spectroscopy (XPS) of both surfaces in UHV. (c) XPS spectra from both the top and substrate of each delaminated sample, establishing that the devices delaminate at the weakly bonded organic monolayer. Examination of the Pt, Si, and Au spectra confirm that the samples split above the substrate/organic interface. The Ti spectra show that >90% of the Ti remains on the top, suggesting that the splitting occurred below the Ti/organic interface. The carbon spectra show a ~50/50 division between the substrate and top, indicating delamination within the monolayer or alternatively a patchlike division of the monolayer to the top and substrate.

and C spectra for each delaminated "top" and "substrate" pair in Figure 1c immediately establishes that every sample delaminated at the organic layer; Au and Si photoelectrons are only seen from the substrate half, and a weak Pt signal from the delaminated top is consistent with photoemission from the top Pt through the Ti and C layers. Titanium is predominantly found on the top sample half, with <10% of the total Ti (by raw XPS counts) on the substrate in the case of Au and Si, and only 2% of the total Ti attached to the PtO_2 substrate. The carbon of the LB monolayer appears ~50/50 split between top and bottom halves, except for the Si case where it preferentially remains ~65/35 attached to the top interface.

In Figure 2, we validate the UHV delamination process through a direct comparison to ion-milled spectra. We examine the Ti/monolayer/Pt sample augmented with an additional 5-nm Ti top capping layer. During one week of air exposure, TiO_2 formed on the cap surface. XPS of this exposed surface shows a clear signature of TiO_2 (Ti^{4+}). Even the most minimal ion milling quickly reduces the TiO_2 into a series of suboxides with lower valence states (Ti^0, Ti^{2+}, and Ti^{3+}), destroying the chemical information. The critical Ti/organic interface is buried under 50 nm of Pt. Ion milling through the sample to this interface again yields a messy spectrum of mixed Ti valence, very similar to the ion-milled surface spectrum. In stark

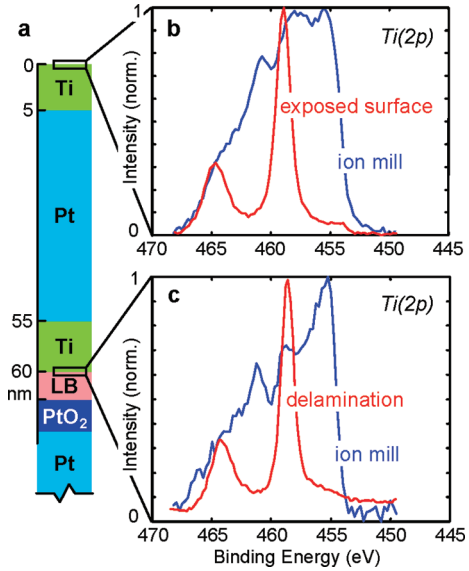

Figure 2. UHV delamination preserves chemical bonding information; ion milling destroys it. (a) Schematic of the Pt/organic monolayer/Ti junction. The key Ti/organic interface is 60 nm below the surface. A Ti-capping layer has been added to this sample. (b) XPS (normalized) for the ambient-exposed Ti surface shows almost pure TiO_2. Minimal Ar ion milling dramatically changes the Ti spectrum by reducing the Ti oxides. (c) The buried Ti/organic interface. Delamination XPS shows predominantly TiO_2 at the interface; the ion-milling spectrum obtained from the same vertical location in the same sample shows a mess of heavily reduced Ti oxides.

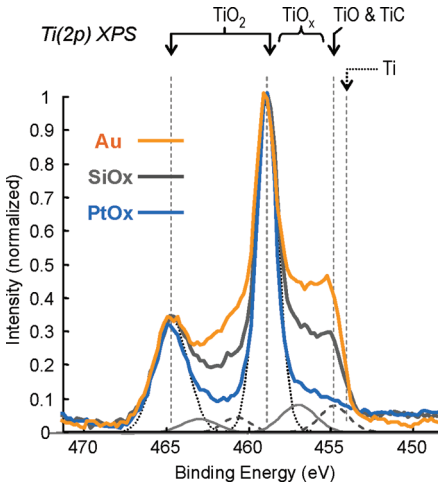

Figure 3. Ti(2p) XPS spectra from the "top" interface of the three structures show significant differences in the chemical composition of the buried Ti film. TiO_2 predominates, but the relative amount of TiO_x and TiC varies substantially. The Au substrate shows the most TiO_x and TiC; the PtO_2 substrate shows the least. SiO_2 falls between the others (in gray: Gaussian doublet peak fits for Ti−O_2 at 458.6 eV, Ti−O_x at 456.8 eV, and Ti−C at 454.7 eV) (Ti = 454.0 eV).

constrast, the UHV delamination spectrum from the same interface of the same sample is dominated by a clean TiO_2 (Ti^{4+}) doublet. It is clear in this case that ion milling destroys the chemical bonding information, whereas UHV delamination preserves it.

To understand the critical Ti/organic interface, Figure 3 focuses on the Ti(2p) spectra acquired from the delaminated "top" of each sample. Peak assignments are shown above the spectra (Ti = 454.0 eV, TiO/TiC = 454.7 eV, TiO_2 = 458.6 eV).[36] In a comparison of the Au, SiO_2, and PtO_2 spectra, two features are immediately evident: (i) all spectra show a majority of titanium oxide species (TiO_2, TiO_x, and TiO), a minor amount of TiC, and no metallic Ti; and (ii) the relative proportion of TiO_2 vs (TiO_x, TiO, TiC) is substrate-dependent, and the most TiO/TiC is found on the Au substrate. In contrast, the PtO_2 substrate shows the most TiO_2 and the least TiO_x, TiO, and TiC. The amount of TiO_2 thus varies as $TiO_{2-PtO2} > TiO_{2-SiO2} > TiO_{2-Au}$. The amount of TiO/TiC follows exactly the opposite trend, with $TiC_{Au} > TiC_{SiO2} > TiC_{PtOx}$.

In contrast, examination of the Ti spectra from the delaminated bottom half "substrate" (Figure 1) shows only TiO_2, no TiO nor TiC. Angle-dependent data (not shown) further establishes that all the TiO_2 rests above the C on these samples; it has not penetrated the LB film to the substrate on any macroscopic level. We tentatively conclude that the samples have delaminated in a "patchwork" fashion with a small amount of TiO_2 adhering to the substrate but most remaining attached to the top electrode. We thus turn to a more detailed analysis of the top Ti and C spectra.

The undistorted XPS spectra acquired from the pristine delaminated surfaces enable reliable quantification of the interface chemistry. Angle-dependent photoemission (ADXPS) in principle enables a depth profile of these species to be constructed. Figure 4a presents the Ti(2p) angle-dependent data for the sample top delaminated from the Au/LB substrate. In Figure 2, this Au sample showed the highest proportion of TiO/TiC as a broad low-binding energy shoulder on the main TiO_2 peak. In Figure 4a, we see that this shoulder is strongly angle-dependent, growing stronger with increasing electron takeoff angle. In this work, the takeoff angle is measured with respect to the sample surface, as illustrated in Figure 4a; higher angles therefore allow emission from materials deeper beneath the surface. The increasing TiO/TiC shoulder on the normalized TiO_2 peak indicates that the TiO/TiC species are located further from the surface than the TiO_2 species. In Figure 4b, we similarly examine the angle-dependent C(1s) spectra of this same Au sample. The carbon spectrum consists of one main peak at 284.8 eV, assigned to the C−C bonds of the LB monolayer, and two small satellite peaks at 288.8 eV, assigned to C−O bonding, and 281.8 eV assigned to carbide C−Ti bonding. Under close examination, the C−Ti peak shows the same strong angle dependence that the TiO/TiC peak did; namely, it grows stronger with increasing emission angle indicating a buried species. By plotting the atomic concentration of each Pt, Ti, O, and C species as a function of emission angle, a qualitative depth profile rapidly emerges, as illustrated in Figure 4c. The exposed interface is dominated by the C−C species, as expected, and thus the relative C−C atomic concentration *decreases* with higher angles. The Pt overlayer signal grows very quickly with increasing angle, putting it, as expected, furthest from the surface. In between, the three Ti species separate cleanly into a TiO_2 band closer to the carbon interface and a TiO/TiC band closer to the Pt overlayer. This layer segregation is independently supported by the angle dependence of the C−Ti signal, which lies close to the Ti−O and Ti−C trends. The oxygen follows a trend midway between the TiO_2 and TiO/TiC; it is clearly present throughout the Ti layer. The schematic on the right side of Figure 4c shows this simplified layer structure: the residual LB carbon at the delaminated interface, above which is fully

(36) *NIST X-ray Photoelectron Spectroscopy Database 20*, version 3.4 (Web version); Wagner, C. D., Naumkin, A. V., Kraut-Vass, A., Allison, J. W., Powell, C. J., Rumble, J. R., Eds.; National Institute of Standards and Technology: Gaithersburg, MD, 2003.

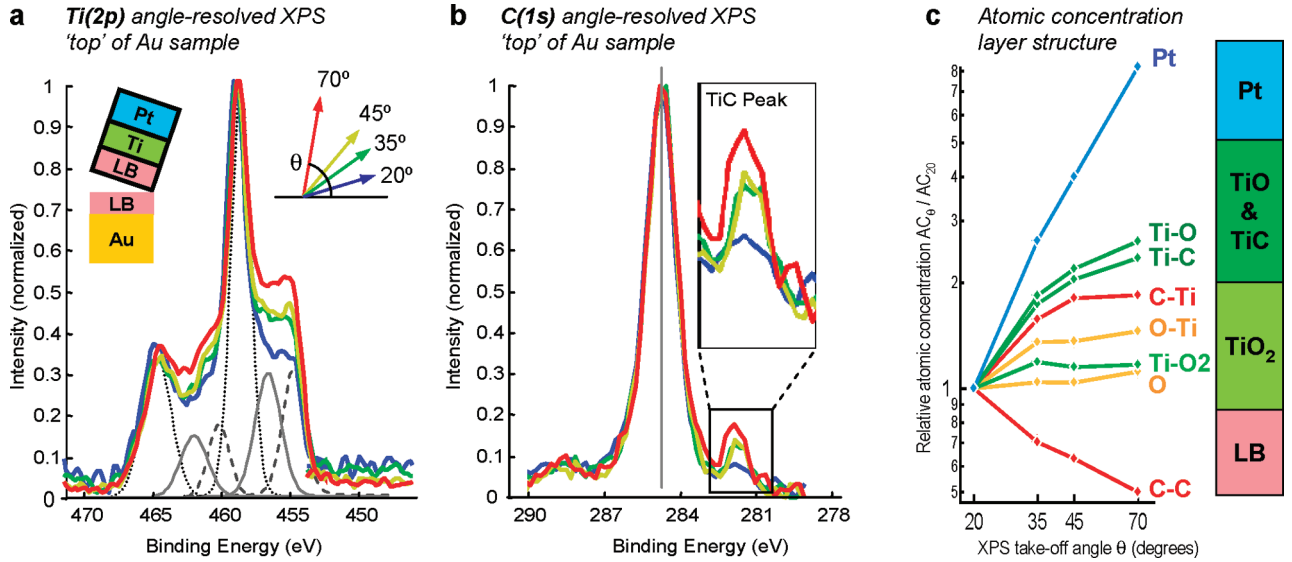

Figure 4. (a) Ti(2p) angled dependent ADXPS spectra from the delaminated "top" surface of the Au substrate sample show an unexpected trend: the TiC and TiO peaks increase with XPS takeoff angle, indicating they are buried below the TiO_2 (in gray: Gaussian doublet peak fits for Ti−O_2 at 458.6 eV, Ti−Ox at 456.8 eV, and Ti−C at 454.7 eV) (Ti = 454.0 eV). (b) C(1s) ADXPS shows the same trend for the TiC peak. (c) Quantification of atomic concentrations as a function of angle enables a simplified layer model to be constructed. Plotted are the relative atomic concentrations ACθ/AC20. The LB film is identified with the surface C−C carbon signature; the Ti oxide and Ti carbide are visible in the Ti(2p) spectra (Ti−O, Ti−C, Ti−O_2), the carbon C(1s) spectra (C−Ti), and the oxygen O(1s) spectra (O, O−Ti). The Pt(4f) signal is from the Pt-capping layer. In particular, this atomic concentration dependence confirms that the TiO_x and TiC reside above the TiO_2 in the fabricated structure. Corresponding data from the SiO_2 and PtO_2 substrates show the same layer structure and are provided in the Supporting Information.

oxidized TiO_2, above which is TiC and partially oxidized TiO_x, finally capped by the Pt overlayer. This same simplified layer structure is found in all three samples (Supporting Information Figure S1).

Establishment of the qualitative chemical interface structure in Figure 4c enables an effort to quantify the relative abundance of each species, taking into consideration attenuated photoemission from the buried layers. The attenuation of a photoemission signal from a substrate of species B due to an overlayer of species A is well-known:[37]

$$I_B = I_B^{\infty} * \exp[-d_A/\lambda_A^B \sin(\theta)] \quad (1)$$

where I_B^{∞} is the intensity from the substrate without an overlayer, d_A is the overlayer thickness, λ_A^B is the electron attenuation length for B photoelectrons in material A, and θ is the emission angle with respect to the surface plane. Similarly, the photoemission signal from the overlayer is self-attenuated as

$$I_A = I_A^{\infty} * \{1 - \exp[-d_A/\lambda_A^A \sin(\theta)]\} \quad (2)$$

where λ_A^A is the electron attenuation length for A photoelectrons in material A. Although the absolute intensities I_A^{∞} and I_B^{∞} are experiment-dependent and thus normally unknown, XPS "sensitivity factors" for each species give their ratio. The two equations can then be solved for the thickness d, and in the case that the A and B photoelectrons are close in energy, $\lambda_A^B \approx \lambda_A^A = \lambda$, further simplification yields[37]

$$d = \lambda \sin(\theta) \ln[1 + (I_A/I_A^{\infty})/(I_B/I_B^{\infty})] \quad (3)$$

$$d = \lambda \sin(\theta) \ln[1 + AC_A/AC_B] \quad (4)$$

where AC_A is the uncorrected atomic concentration of species A. For the case of a finite substrate layer of thickness d_B, similar algebra yields

$$d_A = \lambda \sin(\theta) \ln\{1 + AC_A/AC_B * [1 - \exp(-d_B/\lambda \sin(\theta))]\} \quad (5)$$

Using eqs 4 and 5 and the 45° species-segregated atomic concentrations, we calculate the layer thicknesses for the residual LB monolayer, the entire Ti-containing layer, and separately, the TiO_2 layer and the TiO/TiC layer. It is clear that this quantification rests on the assumption of a discrete layer structure; a second-order model would incorporate overlapping distributions of the TiO_2 and TiO/TiC species. A patchwork distribution of the LB monolayer on the two sides of the delaminated interface would increase layer thickness errors. We also neglect hydrogen and other low cross-sectional elements that do not show in photoemission. The data, however, do not seem to justify further modeling complexity. The primary analysis goals are relative species locations and abundances; calculated results from the first-order layer model are listed under "Ti(2p) analysis" in Table 1.

Figure 5 illustrates these calculated layer thicknesses, and for the case of the PtO_2 substrate, compares them to a cross-sectional transmission electron micrograph (TEM) of a nominally similar sample. The substrate electrode was thinned for the purposes of TEM sample preparation; the nominal structure is Si/native SiO_2 1.5 nm/Ti 3 nm/Pt 6 nm/PtO_2 2.5 nm/LB/Ti 5 nm/Pt 100 nm. Visible in the TEM image is a ~6-nm band of light contrast that includes the residual monolayer and any Ti species, sandwiched on both sides by the dark contrast Pt layers. Visible within this is a thin <2-nm lighter contrast band at the lower Pt surface; this is located where the 2.5-nm LB monolayer is expected. The total 6−7-nm thickness appears in good agreement with the calculated 3.5 nm TiO/TiC + 1.9 nm TiO_2 + 2 nm LB for this PtO_2 substrate.

(37) Cumpson, P. J.; Seah, M. P. *Surf. Interface Anal.* **1997**, *25*, 430.

Table 1. Carbon and Titanium Layer Thicknesses Calculated from the Attenuation-Corrected Photoemission Spectra of All Three Substrates, Using the Stratified Layer Structure of Figure 2c[a]

	Ti(2p) analysis			C(1s) analysis			
substrate	TiO_2 (nm)	TiO_x & TiC (nm)	total Ti oxide[b] (nm)	residual LB monolayer (nm)	C–Ti/C–C ratio	# of carbide atoms from C18	ATR-IR results[c]
Au	0.8	3.9	4.8	1.1	0.09−0.25	1.6−4.5	4.0
SiO_2	1.1	4.1	5.3	1.1	0.08−0.22	1.4−4.0	2.9
PtO_2	1.9	3.5	5.5	1.0	0.03−0.08	0.5−1.4	0.9

[a] The calculation methodology is detailed in the text. The C−Ti/C−C ratio assumes a ∼50/50 split of delaminated carbon between top and substrate surfaces, as supported by the calculated residual LB monolayer thickness. Low carbide estimates assume the TiC is located at the TiO_2/TiO_x interface; high estimates assume the TiC is distributed throughout the TiO_x layer and therefore it sees additional attenuation. Also quoted for reference are results from an independent in situ attenuated total reflection infrared (ATR-IR) spectroscopy investigation of these same samples. [b] The total Ti oxide thickness (all species) is not simply the sum of the TiO_2 and TiO layer thicknesses; it is instead calculated independently as a consistency check. [c] See ref 7.

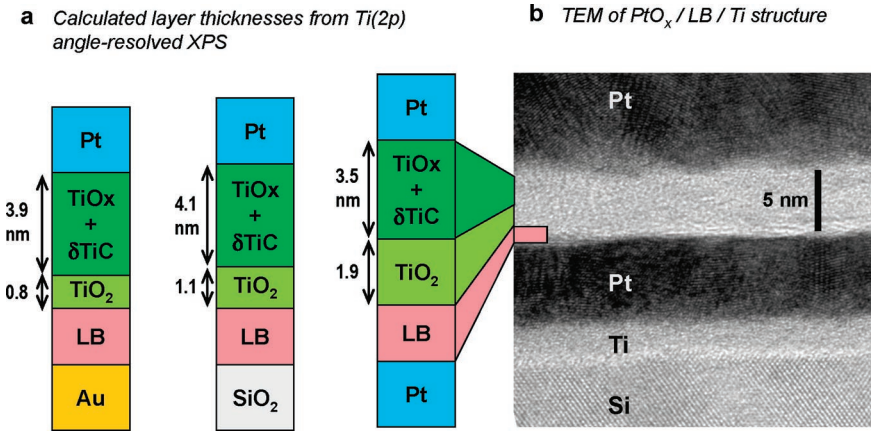

Figure 5. (a) Stratified layer thicknesses calculated from the attenuation-corrected photoemission signals (Table 1). The Au substrate shows a thin 0.8-nm TiO_2 layer and a thicker 3.9-nm TiO_x/TiC layer. The SiO_2 substrate is similar. In contrast, on the PtO_2 substrate twice as much of the Ti is fully oxidized TiO_2. TiC is present in minimal amounts, and hence it is labeled δTiC. (b) TEM of a PtO_2/LB/Ti device structure, as fabricated. The residual monolayer appears as a line of light contrast as indicated. Note for TEM analysis a thinner substrate structure was employed; this PtO_2 device was built on top of a Si/native SiO_2/Ti 3 nm/Pt ∼6 nm/PtO_2 2.5 nm substrate instead of the previous SiO_2 100 nm/Pt 100 nm/PtO_2 2.5 nm substrates.

A final goal of the analysis is to quantify the amount of carbide formed in the Ti/organic reaction. This somewhat risky analysis requires we further assume that the layer structures derived above are correct; we proceed with this caveat. Unfortunately, in the Ti(2p) spectra the TiC and reduced TiO peaks overlap directly. We consequently turn to examination of the C(1s) spectra and particularly the C−C and C−Ti atomic concentrations. From the layer structure, it is clear that the C−C photoelectrons are emitted directly from the sample surface, whereas the C−Ti photoelectrons will be heavily attenuated by the intervening TiO_2 and LB layers. Using eqs 1 and 2 and the approximate titanium layer thicknesses of Table 1, we extract the C−Ti/C−C ratio as corrected for this attenuation; these results are listed as "C(1s) analysis" in Table 1. The largest expected error is the unknown location of the TiC within the layer structure; we therefore calculate a lower bound by assuming that the TiC is found only at the TiO_2/TiO_x interface, and an upper bound by assuming that it is uniformly distributed (intermixed) within the TiO_x layer. A final correction considers the result (Figure 1) that approximately 50% of the LB carbon appears on each half of the delaminated top and substrate. We find that up to 15−20% of the carbon reacts to form carbide for the Au and SiO_2 substrates, and remarkably, on the PtO_2 substrate only <5% of the LB carbon forms TiC. This XPS analysis appears in good agreement with an independent in situ infrared spectroscopy investigation of similar samples.[7]

Discussion

Three results stand out from the above analyses: (1) Ti oxide dominates; surprisingly little TiC forms on *any* of the three substrates, (2) the thickness of the TiO_2 is directly proportional to the amount of "available" substrate oxygen and inversely proportional to the amount of TiC, and (3) the TiC that does form appears not at the Ti/organic interface but separated from it by a 1−2-nm TiO_2 layer. We address each of these in turn.

Previous investigations of the Ti/organic monolayer interface have shown a variety of reactivities and reaction products, strongly dependent upon the terminal organic functional group.[6,7,18,19,23,24,26−32] In a recent comprehensive study of a methyl-terminated alkane thiol self-assembled monolayer on a Au substrate, ∼5 nm of condensed Ti (corresponding to ∼20 Ti monolayers, or ∼40 Ti atoms/molecule) reduced infrared absorption by ∼30%, suggesting that ∼30% of the molecule had reacted to form TiC.[32] This deposition was performed at a rate of ∼0.003 nm/s and a background pressure of $\sim 3 \times 10^{-7}$ Torr, meaning that every monolayer of deposited Ti was exposed to ∼25 langmuirs (L) of background gas. Ti(2p) XPS spectra from a similar sample deposited at lower pressure of $<1 \times 10^{-8}$ Torr (0.8 L/Ti monolayer) showed TiC and TiO_x but no TiO_2 and minimal metallic Ti.[32] In that work and others, the formation of Ti oxide species was attributed to the incorporation of background oxygen during deposition.[6,7,30−32] The Ti depositions in our present study were performed at a rate of 0.01 nm/s and

a background pressure of $\sim 1 \times 10^{-6}$ Torr (yielding a similar net 25 L/Ti monolayer). Our control experiments of Ti deposited onto clean Au at these conditions indicate oxygen incorporation at 30−50% of the Ti atomic concentration (i.e., yielding $\sim TiO_{0.5}$; Supporting Information Figure S2). Such a significant oxygen exposure during deposition can account for much of the TiO_x species observed in the current experiment. A high partial pressure of oxygen species such as H_2O or CO may exist in our ambient-opened evaporator and help explain the disagreement between the ∼9% of monolayer carbon TiC formed in this work and the ∼30% previously observed in high vacuum with similar 25 L/monolayer conditions. This oxygen exposure does not, however, explain the *differences* between the three substrates.

The formation of 1−2 nm of stoichiometric TiO_2 at the Ti/organic interface suggests a finite source of oxygen is present at or near this interface before the Ti deposition begins. Three likely sources exist: (i) surface oxide on the underlying substrate, (ii) water trapped within the LB monolayer, and (iii) an initial high partial pressure of ambient oxygen species that are gettered by the deposition itself. A previous detailed study of the Ti/LB/PtO_2 system showed that the deposited Ti fully reduced 2.5 nm of underlying PtO_2.[38] Since the molar volumes of PtO_2 and TiO_2 are nearly identical, this provides enough oxygen to account for the thick ∼2-nm TiO_2 formed upon the PtO_2 substrate. In the case of the Au sample, no surface oxide exists. The SiO_2 substrate is entirely oxide, but normally presumed to be stable. However, Ti is known to reduce SiO_2 upon direct contact because of its greater enthalpy of formation ($\Delta_f H°_{solid}$ [TiO_2] = −944 kJ/mol; $\Delta_f H°_{solid}$ [SiO_2] ≈ −911 kJ/mol) and has even been shown to reduce SiO_2 through an interceding 4-nm HfO_2 or ZrO_2 oxide film.[39] Considering trapped water, all monolayers were deposited as LB films from a water subphase. The methyl-terminated monolayer surface is highly hydrophobic (contact angle > 108°); thus, a negligible amount of water is expected on top of the monolayer. Infrared spectra (not shown) acquired immediately after LB deposition do show a low, broad H_2O resonance; unfortunately, this H_2O resonance is too broad to permit reliable quantification. Extended in-vacuum annealing may help dry the monolayers but is precluded much above 100 °C where desorption of the organic has been observed.[40,41] In all three cases, it seems likely that the initial stages of the Ti deposition will getter oxygen species (H_2O, CO) from the vacuum chamber to reduce the oxygen species partial pressure for later Ti atoms. We attribute the formation of the thin TiO_2 to all three sources: the chamber, the surface water, and particularly to the reduction of the surface oxide for the PtO_2.

The existence of a surface oxygen source obviously modifies the TiC reaction kinetics. This is evident from the low <10% TiC yield and, more dramatically, from the surprising location of the TiC *above* the TiO_2 layer. The TiO_2 formation is strongly favored over the TiC ($\Delta_f H°_{solid}$ [TiC] = −184 kJ/mol), yet the reaction likely requires oxygen ion diffusion through some or all of the organic monolayer to the Ti/organic interface. This process may be slow enough to allow a small amount of TiC to form before oxygen gettering begins in earnest. Subsequent Ti will be driven to react with the available oxygen, with Ti diffusing downward and oxygen likely diffusing upward, to combine and form TiO_2. This diffusion may well displace the TiC, causing it to "float" on top of the steadily thickening TiO_2. The TiO_2 reaction should stop when all available surface oxygen has been used. This kinetic model can also account for the inverse relation between TiO_2 thickness and TiC amount: more surface oxygen will speed the TiO_2 oxidation reaction and thus inhibit less favorable TiC formation.

Conclusions

Ultrahigh vacuum delamination of buried metal/organic interfaces has yielded unperturbed X-ray photoemission spectra and enabled quantitative analysis of the titanium/organic monolayer interface chemistry. In comparison, conventional ion-mill depth profile XPS is shown to chemically reduce the oxide species, destroying the chemical information. Under standard high-vacuum deposition conditions of $\sim 10^{-6}$ Torr, the titanium/organic monolayer interface is dominated by the formation of Ti oxide, with smaller amounts of Ti carbide. This has significant implications for the many titanium-contacted molecular electronic transport measurements already reported in the literature, some of which may need to be reinterpreted. The Ti reaction kinetics are strongly influenced by the availability of oxygen, which is gettered from the deposition ambient and, critically, from the substrate itself. PtO_2 substrates with a ready supply of oxygen showed a 2-nm-thick layer of TiO_2, a 3-nm TiO_x suboxide layer, and minimal <3% TiC, whereas Au substrates with little available oxygen showed half the TiO_2 but three times as much (∼10%) TiC. Differences in TiO_2 formation are attributed to PtO_2 reduction (for the PtO_2 substrate) and to trapped water (in the case of the Au and SiO_2 substrates). Interestingly, the TiC appears to "float" on top of the growing TiO_2 rather than remain bonded at the Ti/organic interface.

Acknowledgment. We gratefully acknowledge R. Kelley of HP Corvallis for expert TEM analysis, and P. Long, Z. Li, R. Walmsley, and P. Kuekes of HP Labs, K.-I. Seo and M. Kelly of Stanford, and M. Stickle for their expert assistance and insightful discussions. We thank the Defense Advanced Research Projects Agency in the United States for partial support.

Supporting Information Available: In Figure S1, X-ray photoemission data from the SiO_2 and PtO_2 samples are plotted and analyzed in a manner identical to that in Figure 2, confirming that all three samples show the same qualitative layer structure and titanium species trends. In Figure S2, we show that Ti evaporated under our experimental conditions ($P \approx 10^{-6}$ Torr, 0.01 nm/s) deposits as Ti oxide, with stoichiometry dependent upon chamber pressure and deposition rate. This material is available free of charge via the Internet at http://pubs.acs.org.

JA710448E

(38) Blackstock, J. J.; Stickle, W. F.; Donley, C. L.; Stewart, D. R.; Williams, R. S. *J. Phys. Chem. C* **2007**, *111*, 16.
(39) Kim, H.; McIntyre, P. C.; Chui, C. O.; Saraswat, K. C.; Stemmer, S. *J. Appl. Phys.* **2004**, *96*, 3467.
(40) Nishida, N.; Hara, M.; Sasabe, H.; Knoll, W. *Jpn. J. Appl. Phys.* **1996**, *35*, L799−802.
(41) Lavrich, D. J.; Wetterer, S. M.; Bernasek, S. L.; Scoles, G. *J. Phys. Chem. B* **1998**, *102*, 3456.